NASA Technical Memorandum 79208

TRAILING EDGE NOISE DATA WITH COMPARISON TO THEORY

W. Olsen and D. Boldman
Lewis Research Center
Cleveland, Ohio

Prepared for the
Twelfth Fluid and Plasma Dynamics Conference
sponsored by the American Institute of Aeronautics and Astronautics
Williamsburg, Virginia, July 23-25, 1979

AIAA 79-1524

TRAILING EDGE NOISE DATA WITH COMPARISON TO THEORY

by W. Olsen and D. Boldman

Lewis Research Center
Cleveland, Ohio

Prepared for the

Twelfth Fluid and Plasma Dynamics Conference
sponsored by the American Institute of Aeronautics and Astronautics
Williamsburg, Virginia, July 23-25, 1979

TRAILING EDGE NOISE DATA WITH COMPARISON TO THEORY

by W. Olsen and D. Boldman

National Aeronautics and Space Administration
Lewis Research Center
Cleveland, Ohio 44135

INTRODUCTION

Turbulent flow in the vicinity of the edge of a surface causes fluctuating forces, which in turn generate noise (refs. 1 and 2). Surface noise from fixed surfaces can be a significant contributor to the total noise of an aircraft and its engines. The fixed surfaces in engine ducts are one example. Another practical example is the STOL aircraft configuration where the flaps of the wing are moved into the large nonuniform turbulent exhaust flow of the engine in order to increase the lift. For the flaps (airfoils) that are wholly immersed in this turbulent flow, surface noise sources tend to be concentrated near the leading edges because of compressibility. On the other hand there are many practical configurations where there is not significant turbulence at the leading edge. In these cases only the trailing edge will produce surface noise. One common example is the STOL aircraft configuration where the engine is mounted over the wing; the finite turbulent engine exhaust is attached to the wing and passes over the trailing edge.

The acoustic spectra for these cases are primarily broadband because the turbulence and the resulting fluctuating lift forces are broadband. For some flow conditions and geometries, feedback caused tones are also evident at a few specific frequencies in the acoustic spectra. Tone-like acoustic spectra can also be produced by the highly ordered turbulence that occurs immediately downstream of a small flow separation region (e.g., a rod or the thin blunt lip of the core nozzle of a coaxial nozzle). "Tone-like" is used here to indicate that the bandwidth of this "tone" is much larger than that of a feedback tone, but much smaller than broadband spectra.

There are several theories to describe the noise generated by turbulent flow at the edge of a semi-infinite plate. According to reference 3, these theories range from empirical (refs. 4 and 5) to fundamental (refs. 6 to 10). None of these theories predict the entire spectra and spatial emission of noise over a large range of velocity. For example, the early theory of Ffowcs-Williams (ref. 6) can only predict the shape of the radiation pattern for edge noise at very low velocity (i.e., as this quantity approaches zero). In spite of this limitation, the constant pattern shape predicted by this early model is often assumed (refs. 11 and 12) to apply at all velocities.

Subsequent theories have not made significant improvements over the early theory of reference 6 in describing edge noise, because they were based upon the Lighthill analogy. As a consequence, the effect of velocity gradients at the trailing edge was not included even though velocity gradients were shown early (ref. 13) to have a profound effect upon the

radiation pattern of jet noise. A recent fundamental theory for leading and trailing edge noise (Goldstein, ref. 10) includes the effect of velocity gradients on the shape of the radiation pattern. This theory predicts that there is a large change in the shape of the radiation pattern as the velocity increases, especially for trailing edge noise.

A comparison was made in reference 10 between the theoretical results of reference 10 for leading edge noise and the leading edge noise data reported in reference 2. This comparison indicated that the predicted shape of the radiation pattern agreed very well with the data. However, the velocity range of the experiment was too small to result in a large enough difference between the high frequency pattern shapes predicted by the theories of references 6 and 10. Therefore, the importance of including the effect of velocity gradients, which is included in the theory of reference 10 but not in the theory of reference 6, cannot be properly proven by using the data from the leading edge experiment.

A better validation can possibly be achieved in a trailing edge noise experiment with a large range of velocity. Unfortunately, the trailing edge noise experiments that have been reported (e.g., refs. 4, 14, and 15) are inadequate for some combination of the following reasons:

(1) The ranges of velocity, frequency and angle were too small.

(2) The geometry did not properly simulate the semi-infinite plate required by the theory, and the nozzle was often large enough to modify the radiation pattern of the sound.

(3) The trailing edge surface noise data reported was contaminated by volume source (jet) noise.

The objective of the study reported herein were to:

(1) Obtain quality trailing edge noise data that are free of the problems described above.

(2) Compare these data to the radiation pattern shapes predicted by the analytical models of references 6 and 10.

(3) Experimentally determine the effect of the following changes in the flow and geometry at the trailing edge on the shape of the radiation pattern: plate length, flow on one side or two sides, sharp or blunt trailing edges.

NOMENCLATURE

c_o	ambient speed of sound, m/s
f	frequency, Hz
h_j	thickness of the flow based on where velocity 1/2 of U_m, m
h_n	nozzle height, m
L	chordwise length of plate scrubbed by flow from nozzle, m
L_c	total chordwise length of plate, m
$OASPL_c$	overall sound pressure level of trailing edge noise, dB (ref. 2×10^{-5} N/m^2)
$(\tilde{p})^2$	rms acoustic pressure, N/m^2

S	fh_j/U_m Strouhal number of flow at trailing edge
SPL	sound pressure level measured, dB (ref. 2×10^{-5} N/m^2)
SPL_c	corrected SPL so it is pure trailing edge noise, dB (ref. 2×10^{-5} N/m^2)
U_m	peak trailing edge velocity, m/s
U_n	nozzle velocity m/sec, m/s
U_o	as used herein $U_o = U_m/2$, m/s
U_t	as used herein $U_t = U_m$, m/s
α	turbulence intensity
θ_e	polar angle, reference to plate exhaust direction, deg
θ_i	polar angle, referenced to nozzle inlet, 180 - θ_e, deg

DISCUSSION OF THEORY

Only two theories for trailing edge noise are discussed here: the early theory of Ffowcs Williams (ref. 6), because it is widely used; and the recent theory of Goldstein (ref. 10), because it is the only one that includes the effect of velocity gradients. These theories will be used to describe the noise emission caused by turbulent flow over the trailing edge of an infinite plate (see fig. 1).

The formulation in reference 6 results in the following simple relationship for the rms acoustic pressure in the far field:

$$(\tilde{p})^2 \propto U_m^5 \, \alpha^2 \underbrace{\sin^2 (\theta_e/2)}_{\substack{\text{shape of} \\ \text{radiation} \\ \text{pattern}}} \tag{1}$$

where: $\theta_e = 180 - \theta_i$, U_m is the maximum velocity component perpendicular to the XZ plane at the trailing edge and is the turbulence intensity. The symbols are defined in the symbol list. The sound pressure level is proportional to 10 $\log_{10}$ $(\tilde{p})^2$. Equation (1) indicates that the shape of the radiation pattern does not change with velocity, and that the direction of the peak noise is upstream ($\theta_e \rightarrow 180^o$). Even though equation (1) is widely used in practice, the assumptions leading to it indicate that it is only applicable for very low velocities.

The theory described in reference 10 accounts for the effects on acoustic emission of velocity gradients at the edge (e.g., fluid shielding, refraction, etc.). Therefore it should be applicable for a large range of velocity. The shape of the radiation pattern can be predicted at any frequency, but only the low and high frequency limits are described by simple relationships. The acoustic spectra, level, and velocity power law could also be predicted, but the inhomogeneous, anisotropic turbulent flow near the trailing edge would have to be measured across the span in detail, and

analytically modeled for use with the theory; this is beyond the scope of this paper. Nevertheless, a sufficient validation of the essentials of this theory can be conveniently made by comparing the data obtained herein with simple relationships established for the shape of the radiation pattern at low and high frequency. Because of the changing velocity, the patterns can be compared at a low and a high Strouhal number. The Strouhal number is defined here as

$$S = \frac{fh_j}{U_m} \tag{2}$$

Where h_j is taken as the thickness of the flow where the velocity is $U_m/2$ (see fig. 1).

At low frequency (low Strouhal number), the shape of radiation pattern is described by

$$(\tilde{p})^2 \propto \frac{\sin^2 (\theta_e/2)}{(1 - (U_t/c_o) \cos \theta_e)^2} \tag{3}$$

At high frequency (high Strouhal number), the shape of the radiation pattern is described by

$$(\tilde{p})^2 \propto \frac{\sin \theta_e \left[\left|\frac{\left(1 - (1 + U_o/c_o) \cos \theta_e\right)}{1 + (1 - U_o/c_o) \cos \theta_e}\right|\right]^{1/2}}{\left(1 - \frac{U_o}{c_o} \cos \theta_e\right)^2 \left(1 - \frac{U_t}{c_o} \cos \theta_e\right)^2} \tag{4}$$

This equation is applicable for

$$\theta_e > \cos^{-1}\left(\frac{1}{1 + U_m/c_o}\right) \tag{5}$$

which is outside of the "zone of silence."

The velocity U_t is the velocity at the trailing edge where the turbulence source is strongest. The turbulence source, as described in reference 10, was evaluated from the limited turbulent flow measurements of the present work (i.e., the mean velocity and turbulence intensity profiles, $U < y, z >$, $\alpha < y, z >$). This evaluation indicated that the turbulence source term is approximately maximum where the velocity is maximum. Thus, for the present work, it is assumed that

$$U_t \cong U_m \tag{6a}$$

The velocity U_o, as defined in reference 10, is difficult to relate to the experiment. In the absence of more insight, the following value is used.

$$U_o \cong U_m/2 \tag{6b}$$

Only the high frequency radiation pattern is affected by U_o, and U_t only affects the low frequency pattern. These velocities are discussed further at the end of this paper.

The "zone of silence," which occurs at small θ_e (eq. (4)), modifies the shape of the radiation pattern through an exponential damping factor (described in ref. 10). However, there will be no need to account for this effect herein, because jet noise contaminates much of the data at small θ_e.

Equations (3) and (4) involve doppler factors of the form $(1 - U/c_o \cos \theta_e)$, which account for the effect of the convection of the turbulent flow relative to the medium. As the velocity at the trailing edge increases, these factors cause the peak of the radiation pattern to move downstream. Notice that the low frequency pattern (eq. (3)) correctly approaches the pattern of the early theory (eq. (1)) as the velocity approaches zero.

The theory indicates that the shape of radiation pattern in independent of the nature of the turbulence that causes the noise; the shape of the pattern depends only on the surface geometry and the flow velocity.

Apparatus and Procedure

Test rig. - The test rig used to obtain the noise data in this paper is shown schematically in figure 2. The rig consisted of the following (proceeding downstream): a flow control valve; a valve noise quieting section; a long straight run of 15 cm diameter pipe; and finally a slot nozzle that was split into two air streams by the test surface plate. The first valve noise quieting element was a perforated plate. Downstream of that there was a large volume no-line-of-sight muffler. None of the data reported herein were affected by internal valve noise, propagated either through the nozzle exit or through the pipe wall.

Surface geometries tested. - The nozzles and surfaces tested are shown in figure 3(a). Table I lists the geometries and nozzle flow conditions tested. The test surfaces were 0.32 cm thick vertical plates of various flow lengths, L, with either sharp or blunt trailing edges. The tongue of the plate (fig. 2, sideview) was inserted into the slot nozzle and split it into two equal slots of 1.3 cm height and 15 cm width. The leading edge of the plate tongue could generate no significant noise with this arrangement because it was located in a region of low velocity and turbulence. A flow blocker was used for most of the data (fig. 3(a)), so that there was flow on only one side of the plate (the side opposite the microphones). The plate had a span of 2.5 m and rested on the ground. Theoretical predictions will be primarily compared with the data from the nominal configuration, which involved flow on one side of a very large (L_c = 2.5 m) sharp-edged plate of short flow length (L = 10.2 cm).

Acoustic instrumentation and data analysis. - The noise data were obtained outdoors with a horizontal circular array of 0.63 cm diameter condenser microphones as shown in figure 2. The microphone arc was centered on the trailing edge of the plate (the noise source location); the arc was in the plane perpendicular to the vertical plate and passing through the center span of the plate. Eleven (11) microphones were placed at a radius of 3.05 m and at various polar angles that ranged from $\theta_i = 20^o$ to 160^o; one additional microphone was also placed at $\theta_i = -90^o$. The angle $\theta_i = 0^o$ corresponds to the nozzle inlet axis. The angle used in the experiment, θ_i, is transformed to the angle used in the theory, θ_e, by $\theta_i = 180 - \theta_e$. The microphone radius used (more than 50 nozzle diameters), insured that the microphones were in the far field.

Urethane foam panels (15 cm thick) were placed on the ground over the whole microphone circle to reduce acoustic reflections. This arrangement resulted in free field data for frequencies above about 250 Hz. The small plate supports did not cause reflections or shielding.

A small high frequency noise source that is uniform with θ_i was used to determine how much trailing edge noise was shielded by the nozzle at small θ_i. These data indicated that there would be no shielding for any configuration tested, except for the short (L = 2.5 cm) blunt end plate at $\theta_i \leq 25^o$. For shorter plates, the range of angle (θ_i) shielded by the nozzle would greatly increase.

The frequency range of the reported data is 100 Hz to 20 kHz. The noise signals were analyzed directly by an automated one-third-octave band spectrum analyzer; the signals were also tape recorded for subsequent narrowband analysis.

Considering the microphone calibrations, periodic checks on the data system, and the data averaging, it was estimated that each one-third-octave band sound pressure level was repeatable from day-to-day to within about ±1 dB. Accuracy is inferred by the fact that jet noise spectra measured with this facility and data system are within 1 dB of published jet noise data.

The sound pressure level spectra (SPL) reported were corrected (ANSI proposal, ref. 18) for atmospheric attenuation (less than 2 dB at 20 kHz) so that the reported data are lossless. The small contribution of background noise was also removed.

The small jet noise contribution to the measured noise was measured separately as described below, and subtracted. The jet noise data were obtained with the configuration shown on figure 3(b). A very large board, of the same L_c and L as the plate, was moved away from the flow so that the flow missed the trailing edge. This configuration resulted in a good approximation of the jet noise contribution (i.e., the jet noise is partially shielded by the plate and there is no surface noise). None of the data reported required more than a 2 dB correction; usually the correction was nearly zero.

The resulting corrected 1/3-octave band data (SPL_c) represent pure trailing edge noise that is generated solely by turbulence near the trailing edge. These are the data reported. The SPL_c data were summed spectrally to produce the overall sound pressure level, $OASPL_c$.

In summary, the SPL_c data reported herein are considered to be pure trailing edge noise, that is accurate, far and free field, and lossless.

Furthermore, these data are sufficient to validate the theory in that the surface is very large, the velocity range is large, and these data cover a large range of frequency and angle.

Velocity measurements. - Limited hot wire velocity survey measurements were made in order to determine the velocity and flow thickness (U_m, h_j) required by the theory. The method used in taking these measurements is exactly the same as that described in reference 16. The results were in excellent agreement with those reported in reference 19 for an equivalent geometry; therefore no details of the hot wire measurements or data are provided herein.

RESULTS

This section is divided into two parts. In the first part, the trailing edge noise data for the nominal configuration are presented. These data are compared with the theoretical predictions of references 6 and 10. Data that show the effect of flow and geometrical variations from the nominal configuration are presented in the second part of this section; these data are also compared with results from the theory.

Nominal Configuration

The nominal configuration, which was used for most of the trailing edge noise experiments, is described in figures 2, 3(a), and table I. The turbulent flow stream was applied to one side of a large plate (L_c = 2.5 m). The plate had a sharp trailing edge and a flow length, L, of 10.2 cm. Hot wire measurements were made of the peak velocity at the trailing edge, U_m. It was found that U_m was essentially the same as the nozzle velocity (i.e., $U_m/U_n = 1$) for this short flow length. Subsequent figures will all report the trailing edge velocity, U_m, even though only U_n was always measured. Trailing edge noise data, SPL_c, were obtained over a large range of nozzle velocities, U_n.

Noise contours. - Contours describing the complete spectral and spatial noise emission, $SPL_c\ \langle f, \theta_i \rangle$, from the trailing edge are shown on figures 4(a) and (b) for two velocities. The SPL_c data have been smoothed to obtain the contour curves. The dotted region on these figures (i.e., at large θ_i and high frequency) indicates where the correction to remove jet noise from the measured data is greater than 2 dB.

This figure is a useful introduction to the detailed acoustic data plots that will follow. From this figure it can be seen that the peak noise region occurs at small θ_i for low velocities, and at large θ_i for high velocities. The frequency of the peak of the spectra (i.e., the dashed locus curve labeled "PEAK") is fairly independent of θ_i.

In subsequent figures, the SPL_c data will be presented as spectra at a polar angle of $\theta_i = 90^o$ and radiation patterns at constant frequency. The presentation of detailed data permits an accurate comparison of the theory and data.

Spectra. - Figure 5 contains plots of the 1/3-octave band spectra at $\theta_i = 90^o$ for several velocities, U_m. The solid curves are smooth curves

drawn through the data. Notice that the shape of the spectra changes with velocity. In particular, the slope at high frequency becomes less steep at high velocity. This change is also evident in the different velocity power laws along lines of constant Strouhal number, shown dashed. Velocity measurements for the nominal configuration indicate that h_j, for use in the Strouhal number, is 1.4 cm, which is very close to the height of the slot nozzle (h_n = 1.3 cm). Data for the radiation pattern will be compared in subsequent figures to the theory at the low and high Strouhal numbers noted on figure 5.

The slashed symbols on figure 5 are data points that are affected by acoustic feedback tones. The narrowband spectra that correspond to the third octave data plotted on figure 5, are shown on figure 6. Feedback tones are quite evident at velocities of 192 and 243 m/s, but not at lower or higher velocities. The SPL_c data for the few 1/3-octave bands that are affected by feedback tones, are not used for the pattern comparisons made herein. Actually, this restriction was not necessary because the theory (ref. 10) indicates that the shape of the radiation pattern for these tones should be the same as for broadband noise. Indeed, the data show that the radiation pattern shape is the same as the pattern shape for the broadband noise. Furthermore, the data verify the expected result that the frequency of the tone does not change with θ_i; this was expected because the source location (the trailing edge) is stationary with respect to the microphone. These same observations about feedback tones were made in reference 2 for a small chord airfoil, which has a vastly different radiation pattern.

Radiation pattern and comparison to theory. - Data showing the radiation patterns at a constant Strouhal number are plotted on figures 7(a) and (b) for a range of velocities. The data points on figure 7(a) shows the measured pattern at S = 0.08; this is the lowest Strouhal number for which quality data could be obtained over a large range of frequency, polar angle and velocity. Figure 7(b) contains similar data for the highest Strouhal number of quality data (S = 1.0). These data show that there is a large change in the shape of the radiation pattern with velocity, U_m.

The shape of the radiation pattern, predicted by the theory of reference 10, is described by equation (3) for a low Strouhal number. For a high Strouhal number, the pattern is described by equation (4). The theoretical patterns for a low Strouhal number are plotted on figure 7(a) for several velocities as solid curves. The solid curves on figure 7(b) describe the theoretical pattern shapes for a high Strouhal number. Since our interest is only in the shape of these curves, the levels of the analytical curves were adjusted for the best overall fit of the data at each velocity.

The shape of the radiation pattern predicted by the theory of reference 6 is described by equation (1). This single pattern shape, which is independent of velocity, is plotted as a dashed curves on figures 7(a) and (b); the levels of these curves were adjusted to agree with the solid curves at $\theta_i = 90^o$.

It is quite apparent that the Goldstein's theory (ref. 10, solid curves) accurately predicts the shape of the radiation pattern as it changes with velocity. The theoretical result from reference 6 (eq. (1), dashed curves) only agrees with data at low velocity and low frequency.

Equation (1) has been used by many investigators (e.g., refs. 11, 12, and 20) to describe trailing edge noise at all velocities even though reference 6 indicated that it should only be applicable at very low velocity. The data herein prove the correctness of that limitation.

The reason for the limited applicability of equation (1) is that it was based upon the Lighthill acoustic analogy, which means that it cannot account for the effect of velocity gradients in the vicinity of the turbulent source at the trailing edge. It should be pointed out that Goldstein was also the first to show analytically (ref. 13) that velocity gradients must be taken into account for jet noise in order to describe correctly the measured overall sound pressure radiation patterns.

Intermediate frequencies. - A numerical solution of the theory in reference 10 is required in order to determine the shape of the radiation pattern at intermediate frequencies. The intermediate frequencies near the peak of the acoustic spectrum (see fig. 5) make the predominant contribution to the $OASPL_c$. It would be useful to have a simple way to estimate the shape of the $OASPL_c$ radiation pattern. A comparison of the pattern shapes at high and low frequency indicates that these shapes are not very different. This suggests that the shape of the $OASPL_c$ pattern might be estimated by a simple arithmetic average of the analytical patterns for high and low frequency. A check of this approximation is made on figure 8, where the data for the $OASPL_c$ pattern are plotted for each velocity. The solid curves are smooth curves drawn through the data. The dashed curves are the result of an arithmetic average of the low and high frequency theoretical pattern shapes from figures 7(a) and (b). The agreement between the $OASPL_c$ pattern data and this simple approximation is excellent.

Notice that the $OASPL_c$ follow a U_m^5 power law at $\theta_i = 90^o$, which is in agreement with equation (1) from reference 6. The variation of the velocity power law with θ_i is due to the fact that the shape of the radiation pattern changes with velocity. The averaged predicted-pattern-shape, multiplied by U_m^5, can be used to estimate the velocity power law variation with θ_i. This simple averaged pattern-shape approach also resulted in a prediction that agreed well with the $OASPL_c$ data for leading edge noise (ref. 2).

Variations from the Nominal Configuration

The data plotted on figures 5 to 8 were for the nominal configuration. It consisted of a very large plate with a sharp trailing edge; turbulent flow on one side of the plate passed over the last 10.2 cm of the plate.

The remainder of the results are concerned with the effect of variations from that nominal configuration upon the noise emission. The variations are listed on lines 2 through 6 in table I. For the first variation (line 2) the plywood extension used in the nominal configuration was removed so that the plate chord, L_c, was very much smaller. The next variation (line 3) is the same as the nominal configuration except that there is flow on both sides of the plate. The last variations (lines through 6) involve changes in the flow length and the effect of a blunt trailing edge. Before these variations are discussed, the symmetry of the noise radiation pattern is considered.

Equation (3) indicates that the pattern shape at low frequency is only affected by U_t. The pattern shapes calculated for $U_t/U_m = 1/2$ and 1 are shown on figure 13. The effect of U_t/U_m on the shape is only apparent at high velocity. Comparing these curves to the data on figure 7(a) indicates that $U_t/U_m = 1$ is a far better choice than $U_t/U_m = 1/2$.

With U_t set ($U_t/U_m = 1$), only U_o/U_m remains to affect the high frequency pattern shape. Comparisons of the theoretical patterns, for $U_o/U_m = 0$, 1/2 and 1 are now made with the data on figure 7(b). The choice, $U_o/U_m = 0$, is inconsistent with the physical model leading to the theory, furthermore, the data shows this choice to be clearly incorrect. The choice of $U_o/U_m = 1/2$ appears to be slightly better than $U_o/U_m = 1$ for the two velocities shown, and better still if the agreements at all velocities are considered.

Only a small part of the theory in reference 10 had to be used herein in order to check its validity. Considerable insight about turbulent noise sources could be acquired by solving the theory of reference 10 numerically for the complete noise emission (spectra, patterns in all planes and at all frequencies, velocity power law and absolute level). This major task would require detailed measurements and analytical modeling of the turbulence parameters required by the theory. The theory accounts for the rapid changes in the turbulent parameters very near the edge, which are the cause of the noise. Nevertheless, detailed measurements would be required in the bulk turbulent flow across the span. Fortunately, the turbulence parameters and spectra in this outer region are much more simply modeled.

CONCLUSIONS

The shape of the radiation pattern for trailing edge noise changes drastically with velocity. Goldstein's theory (ref. 10), which accounts for the effect of velocity gradients at the noise source, accurately predicts the shape of the pattern as it changes with velocity. Large changes in the character of the turbulent flow near the trailing edge affect the level and spectra of trailing edge noise; however, the shape of the pattern is still accurately predicted by this theory.

REFERENCES

1. Goldstein, M. E., Aeroacoustics, McGraw Hill, New York, 1976.

2. Olsen, W. A., "Noise Generated by Impingement of a Turbulent Flow on Airfoils of Varied Chord, Cylinders, and Other Flow Obstructions," AIAA Paper 76-504, July 1976.

3. Howe, M. S., "A Review of the Theory of Trailing Edge Noise," NASA CR-3021, 1978.

4. Hayden, R. E., Fox, H. L., and Chanaud, R. C., "Some Factors Influencing Radiation of Sound From Flow Interaction with Edges of Finite Surfaces," Bolt, Beranek, and Newman, Inc., Cambridge, Mass., BBN-2797, 1976. (NASA CR-145073)

5. Tam, C. K. W. and Yu, J. C., "Trailing Edge Noise," AIAA Paper 75-489, Mar. 1975.

6. Ffowcs-Williams, J. E. and Hall, L. H., "Aerodynamic Sound Generation by Turbulent Flow in the Vicinity of a Scattering Half-Plane," Journal of Fluid Mechanics, Vol. 40, Part 4, Mar. 1970, pp. 657-670.

7. Crighton, D. G., "Radiation from Vortex Filament Motion near a Half-Plane," Journal of Fluid Mechanics, Vol. 51, Part 2, Jan. 1972, pp. 357-362.

8. Amiet, R. K., "Noise Due to Turbulent Flow Past a Trailing Edge," Journal of Sound and Vibration, Vol. 47, Aug. 8, 1976, pp. 387-393.

9. Crighton, D. G., "Radiation Properties of a Semi-Infinite Vortex Sheet," Proceedings of the Royal Society, London, Series A, Vol. 330, No. 1581, 3 Oct. 1972, pp. 185-198.

10. Goldstein, M. E., "Scattering and Distortion of the Unsteady Motion of Transversely Sheared Mean Flows," Journal of Fluid Mechanics, Vol. 91, Part 4, Apr. 1979, pp. 601-632.

11. Fink, M., "A Method for Calculating Externally Blown Flap Noise," NASA CR-2954, 1978.

12. McKinzie, D. J., Burns, R. J., and Wagner, J. M., "Noise Reduction Tests of Large-Scale-Model Externally Blow Flap Using Trailing-Edge Blowing and Partial Flap Slot Covering," NASA TM X-3379, 1976.

13. Goldstein, M. E. and Howes, W. L., "New Aspects of Subsonic Aerodynamic Noise Theory," NASA TN D-7158, 1973.

14. Scharton, T. D., Pinkel, B., and Wilby, J. F., "A Study of Trailing Edge Blowing as a Means of Reducing Noise Generated by the Interaction of Flow with a Surface," Bolt, Beranek, and Newman, Inc., Canoga Part, Calif., BBN-2593, 1973. (NASA CR-132270)

15. Yu, J. C. and Tam, C. K. W., "An Experimental Investigation of the Trailing Edge Noise Mechanism," AIAA Paper 77-1291, Oct. 1977.

16. Olsen, W. A. and Boldman, D., "Preliminary Study of the Effect of the Turbulent Flow Field Around Complex Surfaces on Their Acoustic Characteristics," AIAA Paper 78-1123, July 1978.

17. Goldstein, M. E., "Characteristics of Unsteady Motion on Transversely Sheared Mean Flows," Journal of Fluid Mechanics, Vol. 84, Part 2, Jan. 1978, pp. 305-329.

18. Bass, H. E., and Shields, F. D., "Atmospheric Absorption of High Frequency Noise and Application to Fractional-Octave Bands," NASA CR-2760, 1978.

19. Abramovich, G. N., The Theory of Turbulent Jets, MIT Press, Cambridge, Mass., 1963, pp. 488-489.

20. Olsen, W. and Karchmer, A., "Lip Noise Generated by Flow Separation From Nozzle Surfaces," AIAA Paper 76-3, Jan. 1976.

TABLE I. - SURFACES TESTED

Config. No.	Test description	Plate geometry			Flow on one side of plate or two?	Nozzle velocity, U_n, m/sec
		Flow length, L	Trailing edge	Chord, L_c		
1	Nominal configuration	10.2 cm	Sharp	Large, 2.5 m	One side	91, 122, 152, 192, 243, 300
	Geometrical variation:					
2	Effect of chord, L_c	10.2 cm	Sharp	0.3 m	One side	91, 152, 243
3	Effect of flow on both sides	10.2 cm	Sharp	Large, 2.5 m	Equal on both sides	91, 152, 243
4	Effect of flow length, L	30.5 cm	Sharp	Large	One side	91, 122, 152, 192, 243
5	Blunted, short L	2.5 cm	Blunt	Large	Equal on both sides	91, 152, 243
6	Blunted, long L	30.5 cm	Blunt	Large	Equal on both sides	91, 152, 243

Notes:
1. Turbulence measurements taken for nominal geometry at U_n = 91 m/sec.
2. Jet noise reference runs taken for the above cases.
3. Have narrowband spectra for all cases.
4. Data table of SPL_c spectra available on request.

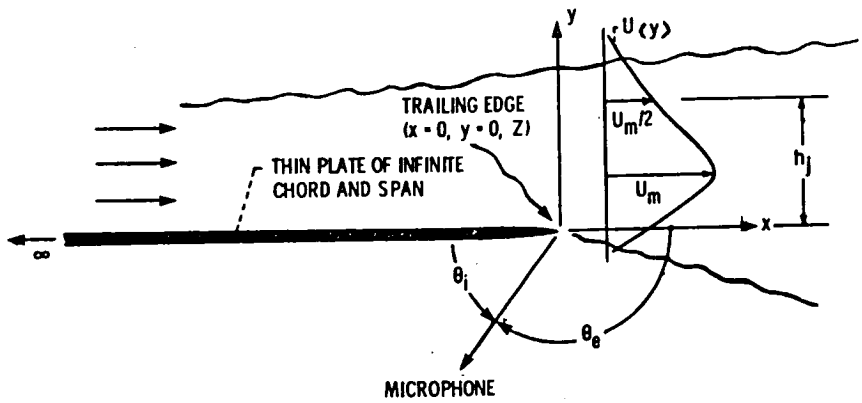

Figure 1. - Turbulent flow over trailing edge of thin semi-infinite plate. Flow of finite extent with arbitrary mean velocity and turbulence gradients.

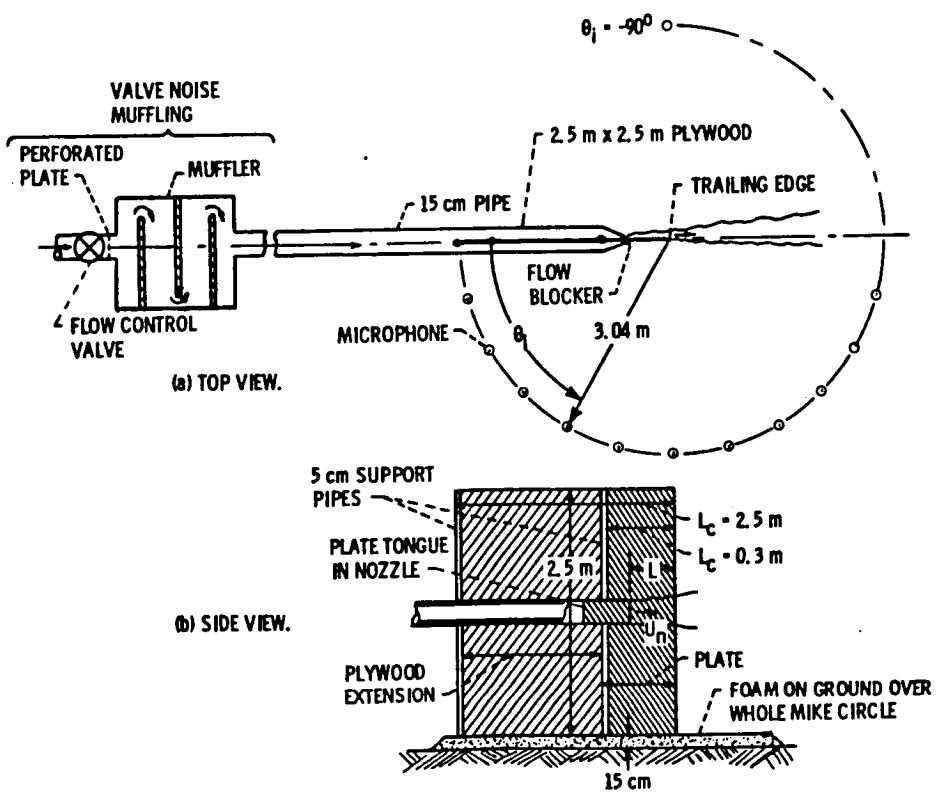

Figure 2. - Flow system, test plate and microphone circle.

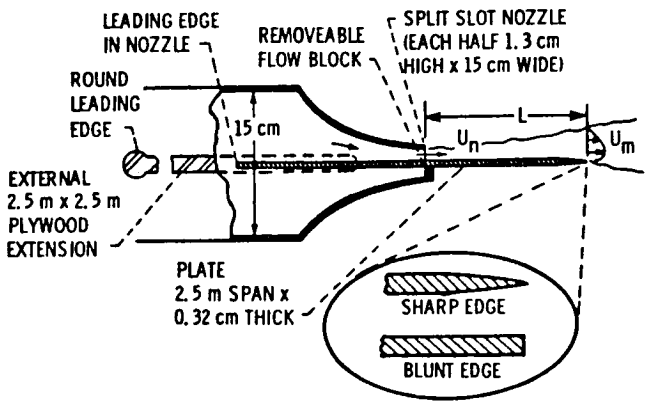

(a) TRAILING EDGE NOISE CONFIGURATIONS.

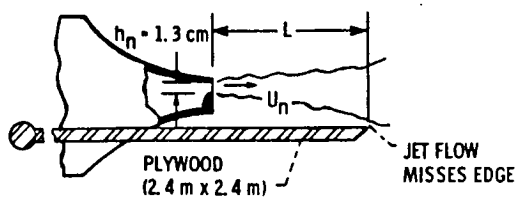

(b) JET NOISE CONFIGURATION.

Figure 3. - Plate - nozzle geometries tested.

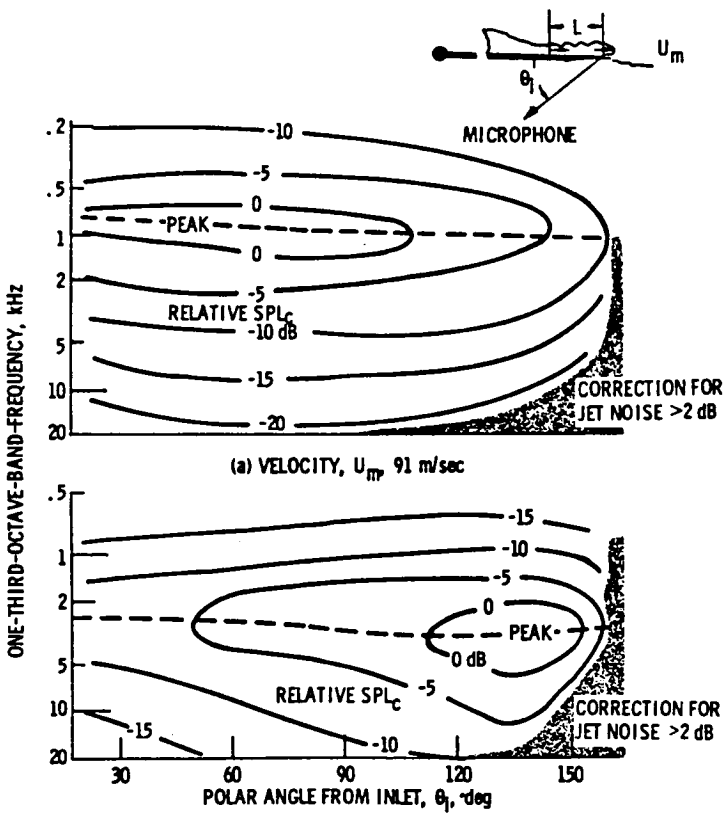

Figure 4. - Smoothed contour plots of noise emission, $SPL_c\langle f, \theta_l\rangle$ for nominal configuration. Semi-infinite plate with sharp trailing edge, and a 2.5 m chord and 2.5 m span; flow length, L, 10.2 cm; microphone circle of radius 3.05 m; microphone plane through center span and perpendicular to plate; data are free-field and lossless (ANSI, ref. 18).

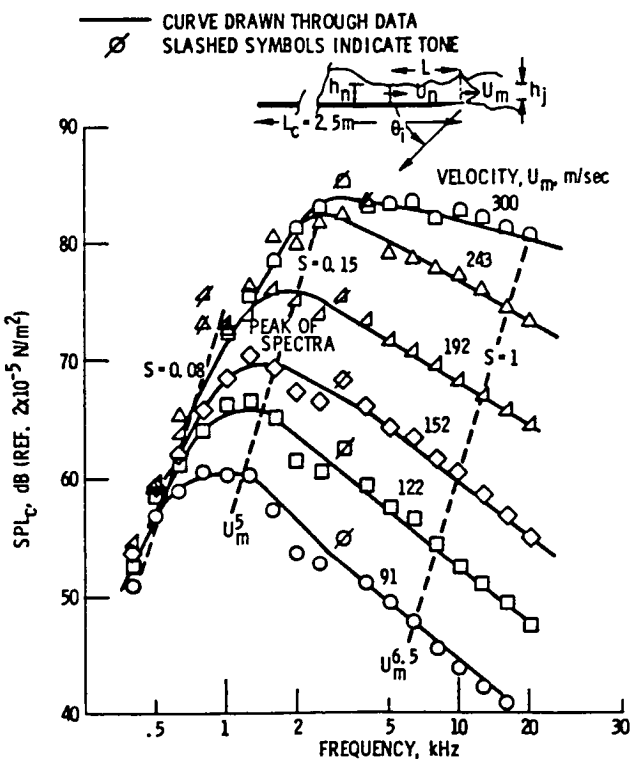

Figure 5. - Trailing edge noise spectra at $\theta_i = 90^0$ for nominal configuration. Semi-infinite plate with sharp trailing edge; flow length, L, 10.2 cm; flow on one side of plate; free field lossless data.

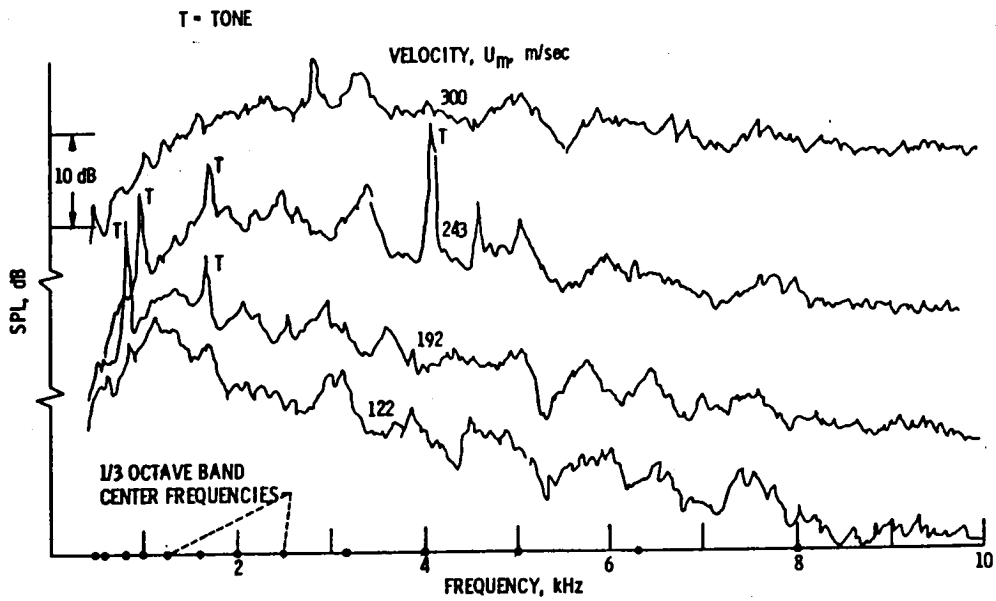

Figure 6. - Narrow band spectra at $\theta_j = 90^0$. Nominal configuration; bandwidth, 30 Hz. Levels adjusted to spread out curves.

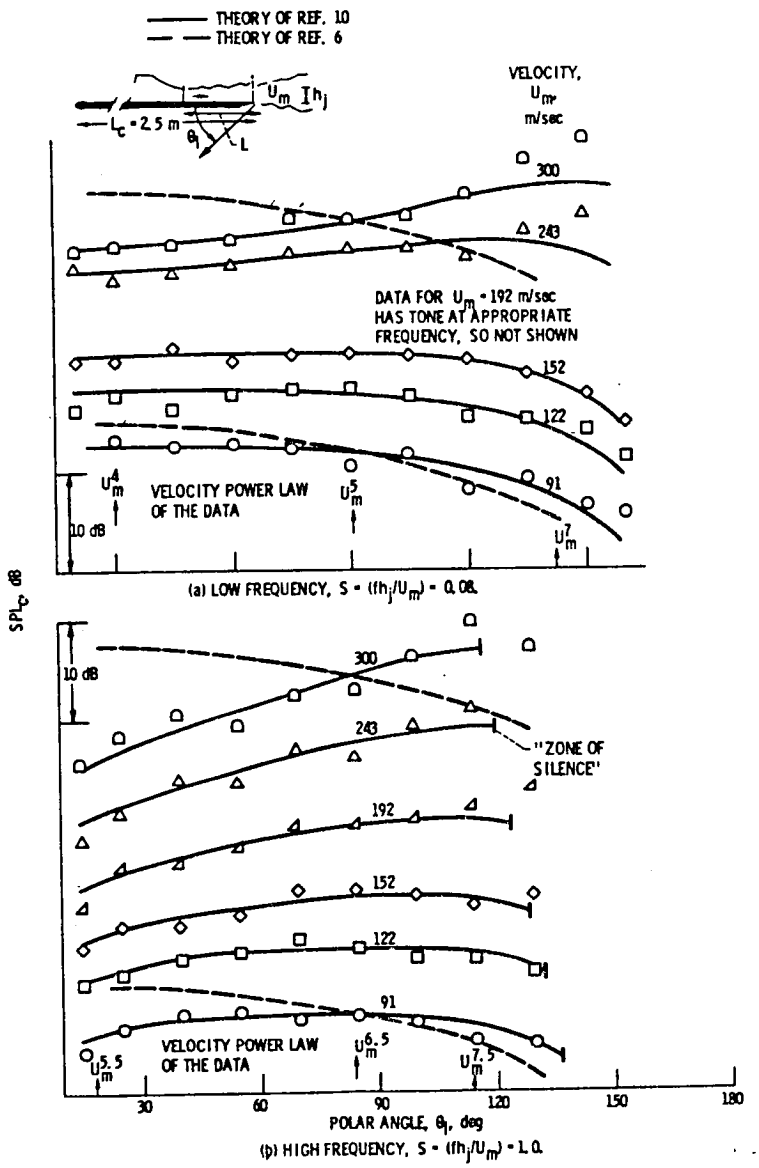

Figure 7. - Trailing edge noise radiation pattern for nominal configuration. Plate 2.5 m x 2.5 m x 0.15 cm with sharp edge; flow length, L, 10.2 cm; flow height at trailing edge, h_j, 1.4 cm; free field lossless data.

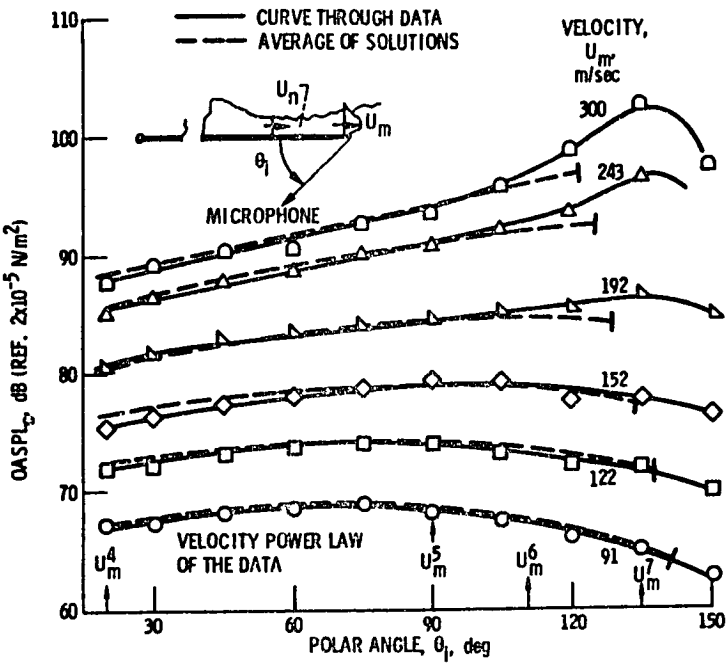

Figure 8. - Overall noise radiation pattern of trailing edge noise nominal configuration. Free field lossless data.

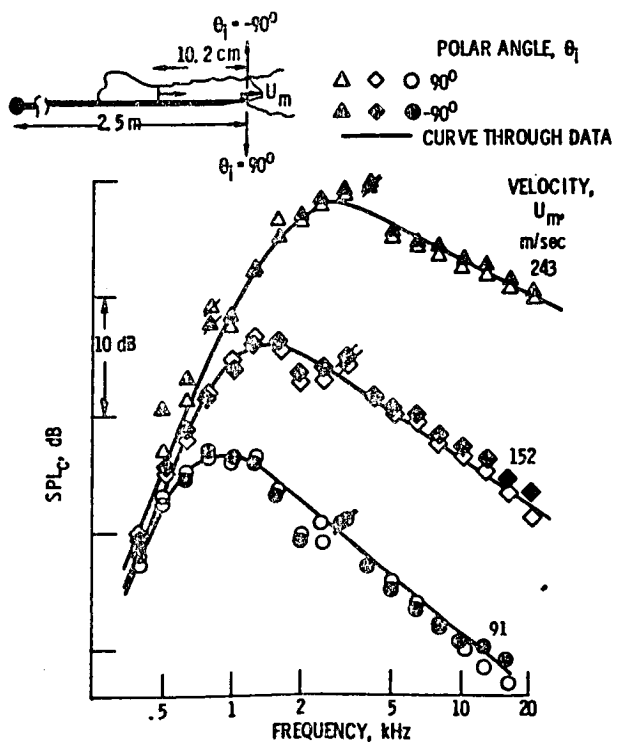

Figure 9. - Symmetry of spectra with flow on one side of plate. Nominal configuration; free field lossless data.

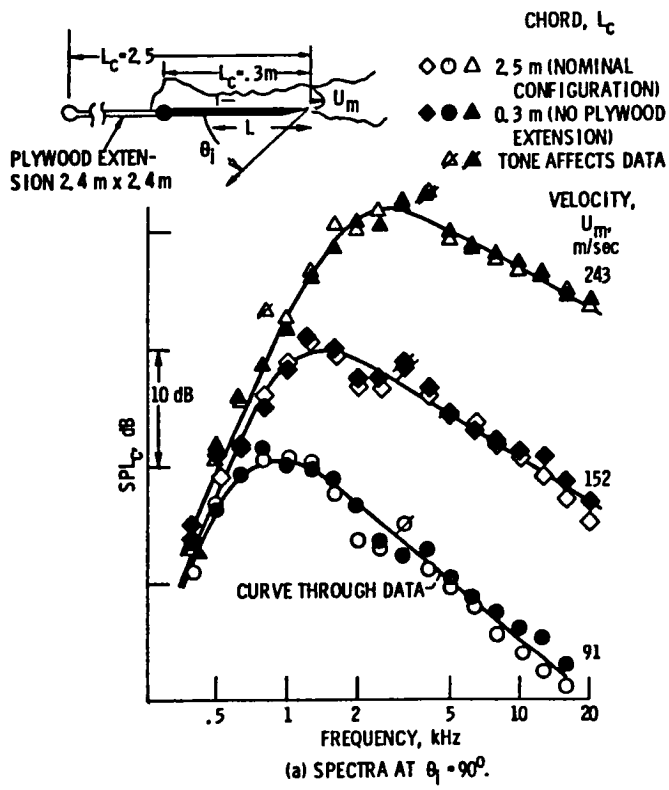

(a) SPECTRA AT $\theta_1 = 90^0$.

Figure 10. - Effect of plate extension upstream of nozzle. Nominal configuration except for chord length, L_c; free field lossless data.

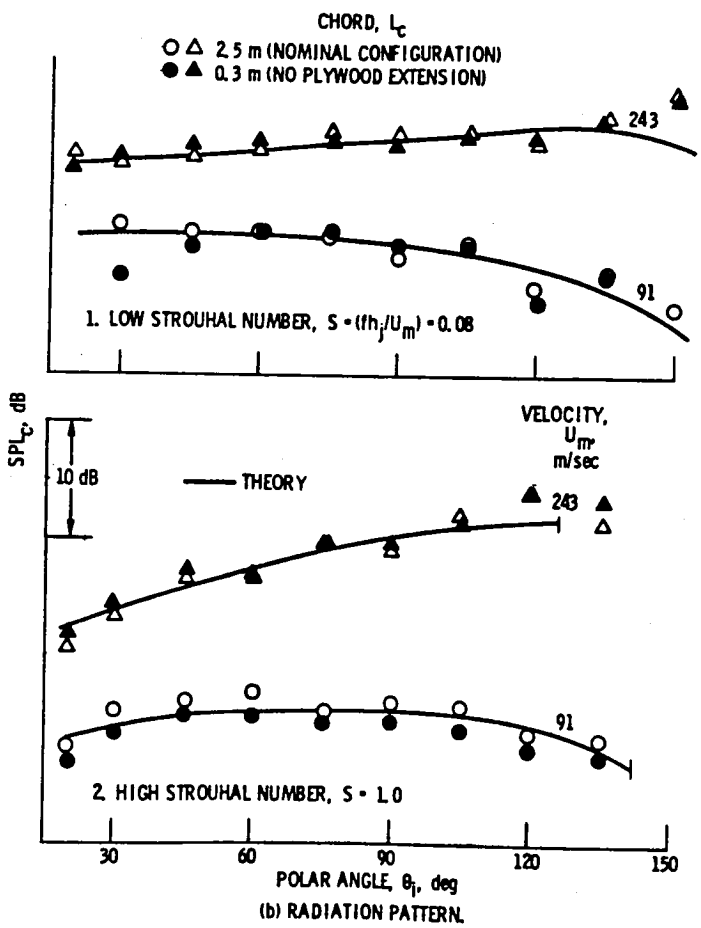

(b) RADIATION PATTERN.

Figure 10. - Concluded.

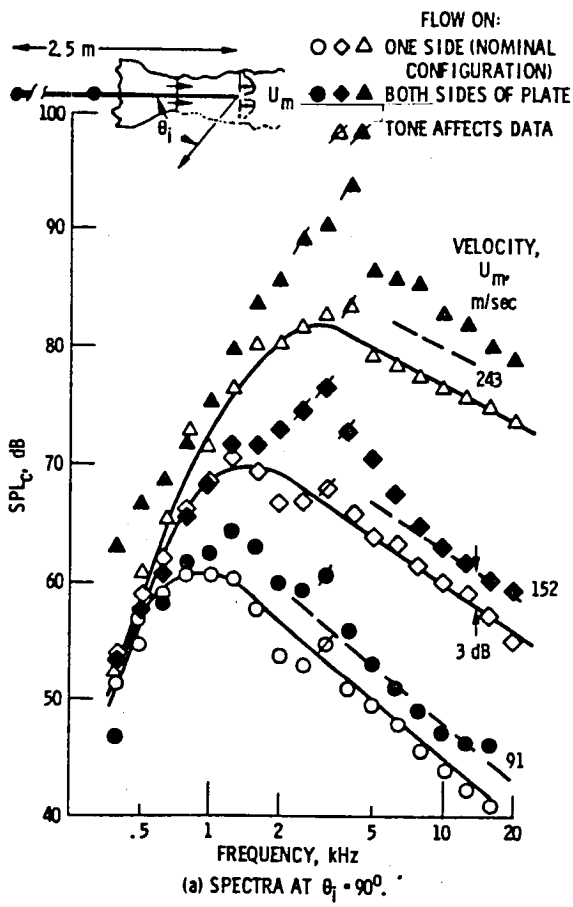

(a) SPECTRA AT $\theta_i = 90^0$.

Figure 11. - Effect of flow on both sides of plate of nominal configuration. Free field lossless data.

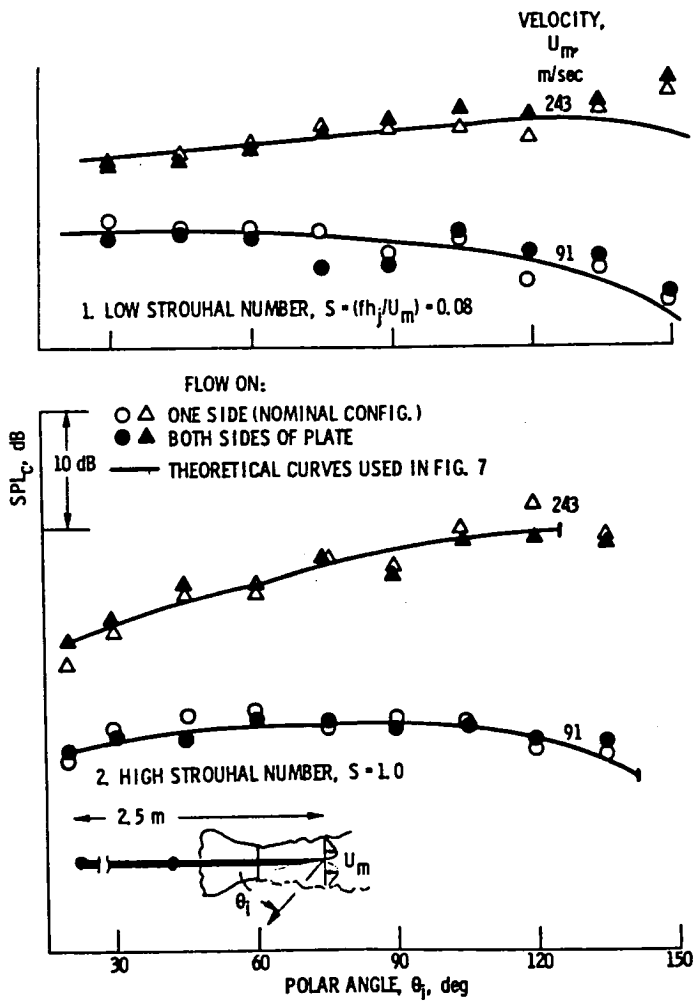

(b) SHAPE OF RADIATION PATTERN (LEVEL ADJUSTED TO SHOW SHAPE).

Figure 11. - Concluded.

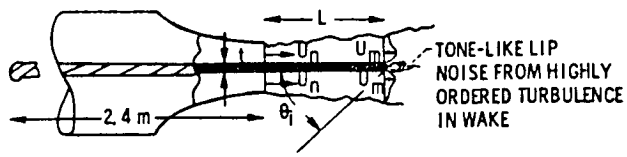

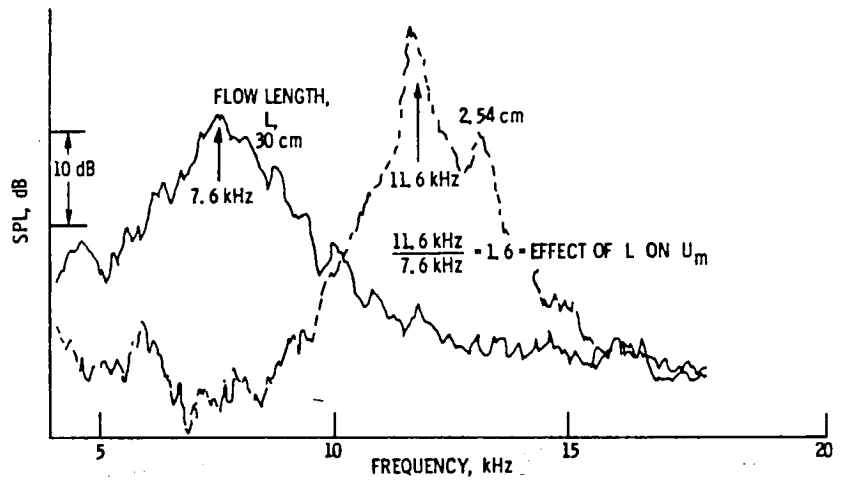

(a) NARROWBAND SPECTRA AT $\theta_i = 90^0$; NOZZLE VELOCITY, U_n, 152 m/sec; BANDWIDTH, 30 Hz

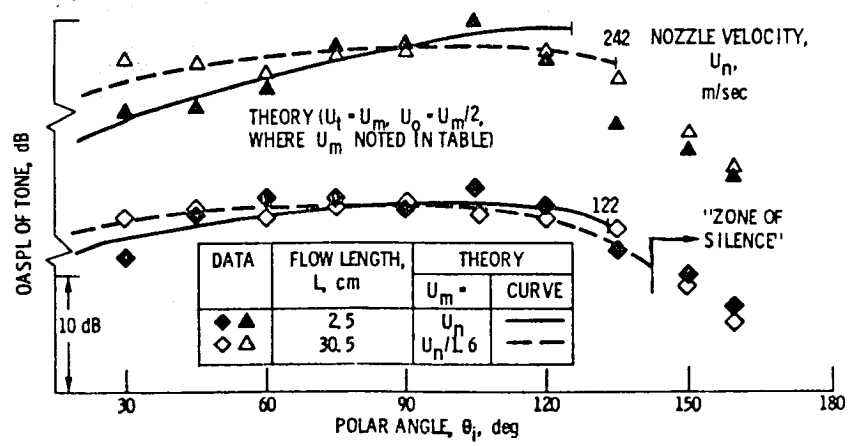

(b) SHAPE OF RADIATION PATTERN OF LIP NOISE (LEVEL ADJUSTED TO COMPARE SHAPES).

Figure 12. - Effect of flow length, L, on lip noise (tone-like trailing edge noise due to flow separation at blunt trailing edge). Blunt ended plate thickness, t, 0.32 cm.

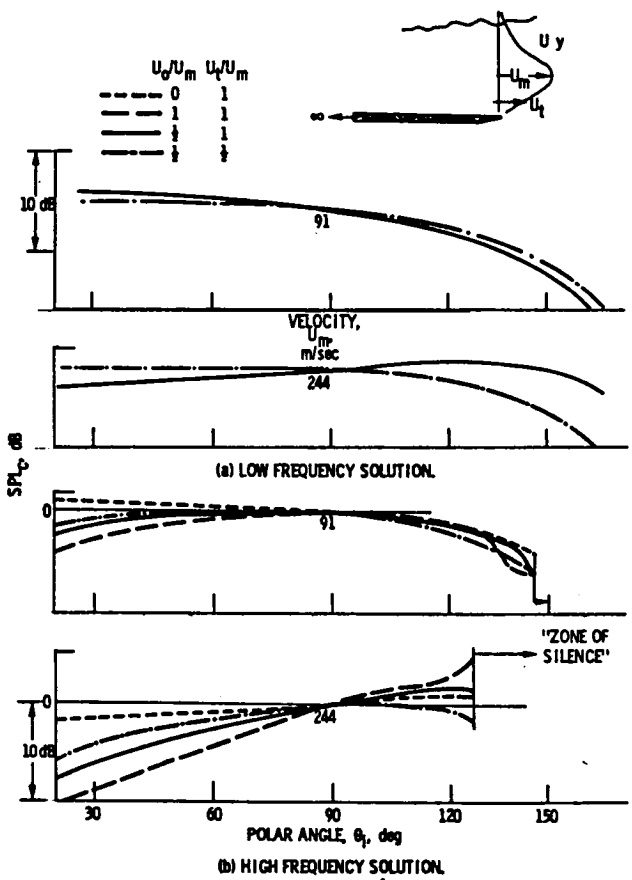

Figure 13. - Effect of flow parameters on the analytical solution for the trailing edge noise radiation pattern.

1. Report No.	2. Government Accession No.	3. Recipient's Catalog No.
NASA TM-79208		

4. Title and Subtitle	5. Report Date
TRAILING EDGE NOISE DATA WITH COMPARISON TO THEORY	6. Performing Organization Code

7. Author(s)	8. Performing Organization Report No.
W. Olsen and D. Boldman	E-093
	10. Work Unit No.

9. Performing Organization Name and Address	11. Contract or Grant No.
National Aeronautics and Space Administration Lewis Research Center Cleveland, Ohio 44135	
	13. Type of Report and Period Covered
12. Sponsoring Agency Name and Address	Technical Memorandum
National Aeronautics and Space Administration Washington, D.C. 20546	14. Sponsoring Agency Code

15. Supplementary Notes

16. Abstract

The noise emission generated by the passage of a turbulent airstream over the trailing edge of a semi-infinite plate was measured over a large range of airstream velocity and plate geometry. The experiment was designed to validate trailing edge noise theories. The results show that the peak of the radiation pattern moves from an upstream to a downstream direction as the velocity increases. The measured radiation pattern of the noise was in excellent agreement with that predicted by the recent theory of Goldstein. As predicted, the pattern shape was independent of the nature of the turbulence producing the noise.

17. Key Words (Suggested by Author(s))	18. Distribution Statement
Aerodynamic noise Trailing-edge flaps	Unclassified - unlimited STAR Category 71

19. Security Classif. (of this report)	20. Security Classif. (of this page)	21. No. of Pages	22. Price*
Unclassified	Unclassified		

* For sale by the National Technical Information Service, Springfield, Virginia 22161

End of Document